Wavelets on Intervals for Image Denoising

Quanhan Li
Dept. of Math.
City University of Hong Kong
Kowloon Tong, Hong Kong
quanhanli2-c@my.cityu.edu.hk

Michelle Michelle
Dept. of Math.
Purdue University
West Lafayette, USA
mmichell@purdue.edu

Bin Han
Dept. of Math. and Stat. Sci.
University of Alberta
Edmonton, Canada
bhan@ualberta.ca

Xiaosheng Zhuang
Dept. of Math.
City University of Hong Kong
Kowloon Tong, Hong Kong
xzhuang7@cityu.edu.hk

***Abstract*—The method of obtaining (bi)-orthogonal wavelets on intervals (boundary wavelets) by a direct approach is employed. The tensor product can then be applied for the construction of high-dimensional boundary wavelets. The ℓ_1 optimization model integrating with such high-dimensional boundary wavelets for regularization was then used for image denoising and can be solved through the ADMM algorithm. Comparisons with the traditional wavelets (without boundary) are done to demonstrate the effectiveness of boundary wavelets and the advantages of the model with ADMM in the presence of large noise levels.**

***Index Terms*—Wavelets on intervals, ℓ_1 optimization model, ADMM, image denoising.**

I. Introduction

The theory of wavelet analysis has received a lot of attention over the past decades, see, e.g., [1]–[8]. Generally, wavelets are functions defined on $L^2(\mathbb{R}^d)$, but in practical applications, such as signal/image processing, data are defined on a bounded domain Ω, e.g., $\Omega = [0, 1]$, the unit interval.

The construction of wavelets on intervals was first given by Meyer [9] in the early 1990s by means of the Gram-Schmidt method. The constructed wavelets on the boundaries, together with those already inside the interval, form the basis of $L^2[0, 1]$. Such approach makes the condition number of orthogonal matrices uncontrollable as the support of the wavelet function increases. To address this problem, Cohen et al. [10] and Andersson et al. [11] give an alternative construction of wavelets on the boundary. After this, a number of pioneers have emerged to contribute to the construction of wavelets on intervals, see, e.g., [12]–[15]. Recently, Han and Michelle [16] provided a general framework for the construction of compactly supported (bi-)orthogonal wavelets on intervals.

Following the construction in [16], [17], we further employ the tensor product to obtain high-dimensional boundary wavelets, which are then integrated into the ℓ_1 optimization model for image denoising. We utilize the ADMM algorithm to solve the ℓ_1-model similar to [18]. We focus on the two-dimensional case that involves large matrix multiplications, which requires a careful algorithmic implementation for the boundary wavelet transforms. To demonstrate the effectiveness of boundary wavelets, we compared the results with those of traditional wavelets under the same soft-thresholding technique. The experimental results demonstrate that the proposed ℓ_1 optimization model with boundary wavelets achieves enhanced performance, particularly at high noise levels ($\sigma \geq 25$). Compared with the commonly used one-step thresholding technique, the solution of the ℓ_1 model through the ADMM method does provide better performance when faced with large noise levels but requires much more computational time.

The structure of the paper is as follows. In Section II, we provide details of the approach for the construction of wavelets on intervals. In Section III, we propose the ℓ_1 optimization model that integrates the boundary wavelets for regularization. In Section IV, numerical experiments on image denoising are performed to demonstrate the effectiveness of the model.

B. Han was supported in part by the Natural Sciences and Engineering Research Council of Canada (NSERC) under grant RGPIN 2024-04991. X. Zhuang was supported in part by the Research Grants Council of Hong Kong (Project nos.: CityU 11309122, CityU 11302023, CityU 11301224) and a grant from the Innovation and Technology Commission of Hong Kong (Project no. MHP/054/22).

II. Boundary (bi)-orthogonal Wavelets on Intervals

A. Han and Michelle's Direct Approach

We present Han and Michelle's recent work that utilizes a direct approach to bi-orthogonal wavelets on intervals without explicitly involving the dual part by constructing wavelets in the half-space $L^2[0, \infty)$ and thus on the interval through symmetric operations and intersection. See [17] for more details.

Define $\Phi_j := \{\phi^L_{j;0}\} \cup \{\phi_{j;k}, n_\phi \leq k \leq 2^j - n_{\mathring{\phi}}\} \cup \{\phi^R_{j;2^j-1}\}$ and $\Psi_j := \{\psi^L_{j;0}\} \cup \{\psi_{j;k}, n_\psi \leq k \leq 2^j - n_{\mathring{\psi}}\} \cup \{\psi^R_{j;2^j-1}\}$, where $f_{j;k} := 2^{j/2} f(2^j x - k)$, while ϕ^L_j and ϕ^R_j are function vectors composed of boundary functions $\{\phi^{L_1}_j, \cdots, \phi^{L_{n_L}}_j\}$ and $\{\phi^{R_1}_j, \cdots, \phi^{R_{n_R}}_j\}$, respectively. Here, n_L and n_R denote the number of functions crossing the left and right boundaries of the interval, and their values are independent of j. Similarly, we can define the wavelet part and even bi-orthogonal counterparts. For the boundary part, the refinement relation should be

$$\phi^L = A_L \phi^L(2\cdot) + \sum_{k \geq n_\phi} a_L(k) \phi(2 \cdot -k), \tag{1}$$

where A_L, A_k are matrices with appropriate sizes, n_ϕ denote the smallest integer such that with $\operatorname{supp}(\phi(\cdot - k)) \subset [0, \infty)$ for all $k \geq n_\phi$.

By [17, Theorem 6.1], for every $J \geq J_0$, one can construct $(\tilde{\mathcal{B}}_J, \mathcal{B}_J)$ that forms a pair of bi-orthogonal Riesz bases of $L^2([0,1])$, where

$$\mathcal{B}_J := \Phi_J \cup \{\Psi_j : j \geq J\}, \quad \tilde{\mathcal{B}}_J := \tilde{\Phi}_J \cup \{\tilde{\Psi}_j : j \geq J\}$$

and there exist (sparse) matrices $A_j, B_j, \tilde{A}_j, \tilde{B}_j$ such that the refinement relations hold:

$$\Phi_j = A_j \Phi_{j+1} \text{ and } \Psi_j = B_j \Phi_{j+1},$$
$$\tilde{\Phi}_j = \tilde{A}_j \Phi_{j+1} \text{ and } \tilde{\Psi}_j = \tilde{B}_j \tilde{\Phi}_{j+1}.$$

Moreover, we have the perfect reconstruction condition:

$$\begin{bmatrix} \tilde{A}_j \\ \tilde{B}_j \end{bmatrix} \begin{bmatrix} \bar{A}_j^\top & \bar{B}_j^\top \end{bmatrix} = I_{\#\Phi_{j+1}}.$$

According to Han's construction, we have $n_{\tilde{\phi}} \geq n_\phi$ and $n_{\tilde{\hat{\phi}}} \geq n_{\hat{\phi}}$. Thus we can define

$$\Phi^L_{J;0} := [\phi^L_{J;0}; \phi_{J;n_\phi}; \cdots ; \phi_{J;n_{\tilde{\phi}}-1}], \tag{2}$$

and

$$\Phi^R_{J;2^J-1} := [\phi_{J;2^J-n_{\tilde{\hat{\phi}}}+1}; \cdots ; \phi_{J;2^J-n_{\hat{\phi}}}; \phi^R_{J;2^J-1}]. \tag{3}$$

Consequently, the projection of a function $f \in L^2([0,1])$ at level J can be represented as

$$f_J = \langle f, \tilde{\phi}^L_{J;0}\rangle^\top \Phi^L_{J;0} + \sum_{k=n_{\tilde{\phi}}}^{2^J-n_{\tilde{\hat{\phi}}}} \langle f, \tilde{\phi}_{J;k}\rangle \phi_{J;k} + \langle f, \tilde{\phi}^R_{J;2^J-1}\rangle^\top \Phi^R_{J;2^J-1}. \tag{4}$$

Using the multi-level relation, the space spanned by Φ_J is the same as the the one spanned by Φ_{J_0} plus $\Psi_j, j = J_0, \dots, J-1$, leading to,

$$f_J = \sum_{\eta \in \Phi_J} \langle f, \tilde{\eta}\rangle \eta = \sum_{\eta \in \Phi_{J_0}} \langle f, \tilde{\eta}\rangle \eta + \sum_{j=J_0}^{J-1} \sum_{\eta \in \Psi_j} \langle f, \tilde{\eta}\rangle \eta.$$

B. Boundary (Bi-)Orthogonal Wavelet Transform

By the refinement relations, we have the decomposition relation between 2 levels for the approximation coefficients:

$$\begin{aligned}\langle f, \tilde{\Phi}_{J-1}\rangle \Phi_{J-1} =& \langle f, \tilde{A}_{J-1}\tilde{\Phi}_J\rangle A_{J-1}\Phi_J \\ =& \langle f, \tilde{\Phi}_J\rangle \left[\overline{\tilde{A}_{J-1}}^\top A_{J-1}\right] \Phi_J.\end{aligned}$$

Similarly, for the wavelet detail coefficients, we have the reconstruction relation:

$$\begin{aligned}\langle f, \tilde{\Psi}_{J-1}\rangle \Psi_{J-1} =& \langle f, \tilde{B}_{J-1}\tilde{\Phi}_J\rangle B_{J-1}\Phi_J \\ =& \langle f, \tilde{\Phi}_J\rangle \left[\overline{\tilde{B}_{J-1}}^\top B_{J-1}\right] \Phi_J.\end{aligned}$$

Therefore, we have

$$\begin{aligned}&\langle f, \tilde{\Phi}_{J-1}\rangle \Phi_{J-1} + \langle f, \tilde{\Psi}_{J-1}\rangle \Psi_{J-1} \\ =& \langle f, \tilde{\Phi}_J\rangle \left[\overline{\tilde{A}_{J-1}}^\top A_{J-1} + \overline{\tilde{B}_{J-1}}^\top B_{J-1}\right] \Phi_J \\ =& \langle f, \tilde{\Phi}_J\rangle \Phi_J.\end{aligned}$$

Define

$$c_j := \langle f, \tilde{\Phi}_j\rangle \text{ and } d_j := \langle f, \tilde{\Psi}_j\rangle.$$

Then, the decomposition from c_J to $\{c_{J-1}, d_{J-1}\}$ is given by

$$c_{J-1} = \langle f, \tilde{A}_{J-1}\tilde{\Phi}_J\rangle = \langle f, \tilde{\Phi}_J\rangle \overline{\tilde{A}_{J-1}}^\top = c_J \overline{\tilde{A}_{J-1}}^\top,$$
$$d_{J-1} = \langle f, \tilde{B}_{J-1}\tilde{\Phi}_J\rangle = \langle f, \tilde{\Phi}_J\rangle \overline{\tilde{B}_{J-1}}^\top = c_J \overline{\tilde{B}_{J-1}}^\top.$$

The reconstruction of c_J from $\{c_{J-1}, d_{J-1}\}$ is given by

$$\begin{aligned}c_J =& c_J \left[\overline{\tilde{A}_{J-1}}^\top A_{J-1} + \overline{\tilde{B}_{J-1}}^\top B_{J-1}\right] \\ =& \left[(c_J \overline{\tilde{A}_{J-1}}^\top) A_{J-1} + (c_J \overline{\tilde{B}_{J-1}}^\top) B_{J-1}\right] \\ =& c_{J-1}A_{J-1} + d_{J-1}B_{J-1}.\end{aligned}$$

C. Examples

In this section we give two most common examples: the Haar and the bi-orthogonal wavelets from the hat function.

Example 1 (The Haar Orthogonal Boundary Wavelets): Consider the compactly supported orthogonal Haar wavelet $\{\phi; \psi\}$ with $a = \{\frac{1}{2}, \frac{1}{2}\}_{[0,1]}$. Recall that $\phi = \chi_{[0,1]}$. Define:

$$\Phi_j := \{\phi_{j;0}\} \cup \{\phi_{j;k} : 1 \leq k \leq 2^j - 2\} \cup \{\phi_{j;2^j-1}\},$$
$$\Psi_j := \{\psi_{j;0}\} \cup \{\psi_{j;k} : 1 \leq k \leq 2^j - 2\} \cup \{\psi_{j;2^j-1}\}.$$

Then $\mathcal{B}_J := \Phi_{J_0} \cup \{\Psi_j\}_{j=J_0}^\infty$, where $J_0 \geq 1$, is an orthonormal basis of $L^2[0,1]$.

Example 2 (Biorthogonal Boundary Wavelets): Consider the scalar biorthogonal wavelet $(\{\tilde{\phi}; \tilde{\psi}\}, \{\phi; \psi\})$ and a biorthogonal wavelet filter bank $(\{\tilde{a}; \tilde{b}\}, \{a; b\})$ given by

$$a = \{\frac{1}{4}, \frac{1}{2}, \frac{1}{4}\}_{[-1,1]},\ b = \{-\frac{1}{8}, -\frac{1}{4}, \frac{3}{4}, -\frac{1}{4}, -\frac{1}{8}\}_{[-1,3]},$$
$$\tilde{a} = \{-\frac{1}{8}, \frac{1}{4}, \frac{3}{4}, \frac{1}{4}, -\frac{1}{8}\}_{[-2,2]},\ \tilde{b} = \{-\frac{1}{4}, \frac{1}{2}, -\frac{1}{4}\}_{[0,2]}.$$

The analytic expression of ϕ is the hat function: $\phi = (x+1)\chi_{[-1,0]} + (1-x)\chi_{[0,1]}$. We denote this wavelet system as **CW** as a classical wavelet system without boundary consideration to be used in the next section.

The primal left boundary elements can be represented as

$$\begin{aligned}\phi^L =& \phi\chi_{[0,1]} = \phi^L(2\cdot) + \frac{1}{2}\phi(2\cdot -1), \\ \psi^L =& \phi^L(2\cdot) - \frac{5}{6}\phi(2\cdot -1) + \frac{1}{3}\phi(2\cdot -2).\end{aligned}$$

For the dual part, we utilize (1) to define $\tilde{\phi}^L$ and $\tilde{\psi}^L$, where

$$\tilde{A}_L = \begin{bmatrix} -\frac{2}{9} & -\frac{2}{36} & \frac{2}{72} \\ \frac{14}{9} & \frac{14}{36} & -\frac{14}{72} \\ -\frac{2}{3} & \frac{4}{3} & \frac{4}{3} \end{bmatrix}, \tilde{a}_L = \begin{bmatrix} \frac{1}{2} & \frac{3}{2} & \frac{1}{2} & -\frac{1}{4} \\ \frac{1}{2} & -\frac{1}{4} & 0 & 0 \\ 0 & 0 & 0 & 0 \end{bmatrix}_{[3,6]},$$
$$\tilde{B}_L = \begin{bmatrix} -\frac{4}{9} & -\frac{1}{9} & \frac{1}{18} \\ \frac{2}{3} & -\frac{4}{3} & \frac{2}{3} \end{bmatrix}, \tilde{b}_L = \begin{bmatrix} 1 & -\frac{1}{2} \\ 0 & 0 \end{bmatrix}_{[3,4]}.$$

The right boundary elements can be defined using symmetry:

$$\phi^R = \phi^L(1-\cdot),\ \psi^R = \psi^L(1-\cdot),$$
$$\tilde{\phi}^R = \tilde{\phi}^L(1-\cdot),\ \tilde{\psi}^R = \tilde{\psi}^L(1-\cdot).$$

Define the generators at scale j by:

$$\begin{aligned}\tilde{\Phi}_j =&\{\tilde{\phi}^L_{j;0}\} \cup \{\tilde{\phi}_{j;k} : 3 \le k \le 2^j - 3\} \cup \{\tilde{\phi}^R_{j;2^j-1}\},\\ \tilde{\Psi}_j =&\{\tilde{\psi}^L_{j;0}\} \cup \{\tilde{\psi}_{j;k} : 2 \le k \le 2^j - 3\} \cup \{\tilde{\psi}^R_{j;2^j-1}\},\\ \Phi_j =&\{\phi_{j;2}, \phi_{j;1}, \phi^L_{j;0}\} \cup \{\phi_{j;k} : 3 \le k \le 2^j - 3\}\\ &\cup \{\phi_{j;2^j-2}, \phi_{j;2^j-1}, \phi^R_{j;2^j-1}\},\\ \Psi_j =&\{\psi_{j;1}, \psi^L_{j;0}\} \cup \{\psi_{j;k} : 2 \le k \le 2^j - 3\}\\ &\cup \{\psi_{j;2^j-2}, \psi^R_{j;2^j-1}\}.\end{aligned}$$

Let $\mathcal{B}_J := \Phi_J \cup \{\Psi_j\}_{j=J}^{\infty}$ and $\tilde{\mathcal{B}}_J := \tilde{\Phi}_J \cup \{\tilde{\Psi}_j\}_{j=J}^{\infty}$. Then $(\tilde{\mathcal{B}}_J, \mathcal{B}_J)$, where $J \ge 3$, is an biorthonormal basis of $L^2[0,1]$. We denote this system as **BW** as a boundary wavelet system to be used in next section.

III. Optimization Model and Algorithms

A. Optimization Model

Given data set $\{(x_i, f(x_i))\}_{i=1}^n$ of samples, and we can approximate f_J as in (4). It is worth noting that in the general case, f_J is only an approximation of f, but for the particular bi-orthogonal wavelet in Example 2, f_J has the interpolation property, i.e., $f_J(x_i) = f(x_i)$ for all i.

Define the matrix according to Φ_j in Example 2:

$$\begin{aligned}\Phi_x :=&[\eta(x_j)]_{\eta\in\Phi_J, 1\le j\le n}\\ =&\begin{bmatrix}\phi_{J;2}(x_1) & \phi_{J;1}(x_1) & \cdots & \phi^R_{J;2^J-1}(x_1)\\ \phi_{J;2}(x_2) & \phi_{J;1}(x_2) & \cdots & \phi^R_{J;2^J-1}(x_2)\\ \vdots & \vdots & \ddots & \vdots\\ \phi_{J;2}(x_n) & \phi_{J;1}(x_n) & \cdots & \phi^R_{J;2^J-1}(x_n)\end{bmatrix}\end{aligned}$$

and $c = [c_{J;2}, c_{J;1}, \dots, c^R_{J;2^J-1}]^\top$. Then we have $f_J = \Phi_x c$. Defien $d_j = B_j c$ for $j = J_0, \dots, J-1$.

This allows us to introduce our ℓ_1 optimization model:

$$\arg\min_c \frac{1}{2}\|\Phi_x c - f_J\|_2^2 + \sum_{j=J_0}^{J-1} \lambda_j \|B_j c\|_1, \tag{5}$$

where λ_j are the regularization parameters. To apply the ADMM algorithm, we define $B = [B_{J-1}; \dots; B_{J0}]$ and λ s.t. $\lambda Bc = [\lambda_{J-1} B_{J-1} c; \dots; \lambda_{J0} B_{J0} c]$.

Define $d = Bc$ and $K(c) = \frac{1}{2}\|\Phi_X c - f_J\|_2^2, H(d) = \lambda\|d\|_1$. Then, (5) is equivalent to minimize $K(c) + H(d)$ s.t. $Bc - d = 0$. Define augmented Lagrangian function:

$$L(c, d; v) = K(c) + H(d) + v^\top(Bc - d) + \frac{\rho}{2}\|Bc - d\|_2^2, \tag{6}$$

where v is a vector and ρ is a constant.

To normalize the vector, let $\mu = \frac{v}{\rho}$, then we have

$$v^\top(Bc - d) + \frac{\rho}{2}\|Bc - d\|_2^2 = \frac{\rho}{2}\|Bc - d + \mu\|_2^2 - \frac{\rho}{2}\|\mu\|_2^2.$$

Thus we can solve the original problem by pairwise iteration:

- $c^{k+1} = \arg\min_c K(c) + \frac{\rho}{2}\|Bc - d^k + \mu^k\|_2^2$,
- $d^{k+1} = \arg\min_d H(d) + \frac{\rho}{2}\|Bc^{k+1} - d + \mu^k\|_2^2$,
- $\mu^{k+1} = \mu^k + Bc^{k+1} - d^{k+1}$,

and this process has the explicit form:

- $c^{k+1} = (\Phi_x^\top \Phi_x + \rho(B^\top B))^{-1}(\Phi_x^\top f_J + B^\top(d^k - \mu^k))$,
- $d^{k+1} = T_{\frac{\lambda}{\rho}}(Bc^{k+1} + \mu^k)$, where T is the soft-thresholding operator,
- $\mu^{k+1} = \mu^k + Bc^{k+1} - d^{k+1}$.

In the first step of the iteration, we update c through an inverse matrix, which may not exist, so instead of this, we use a conjugate gradient to approximate the result.

The convergence of this iterative process is guaranteed in the fulfillment of the KKT condition:

$$-B^\top x \in \partial K(c), x \in \partial H(d), Bc - d = 0, \tag{7}$$

and it can be simplified to the form $-\lambda B^\top \text{sgn}(Bc) = 2^J c - 2^{J/2} f_J$, with a solution c existing.

B. Algorithms

We start with a description of the Algorithm 1 for (S2) the computation of approximation coefficients c_J, (S3) the decomposition of c_J to c_{J-1}, the wavelet coefficients d_{J-1}, (S4) the thresholding of d_{J-1}, and (S5) the reconstruction of the approximation coefficients c_J from c_{J-1} and d_{J-1}.

Algorithm 1 Boundary Wavelet Transforms

(S1) Determine the finest level J. Let f be the input noisy 1-D signal with size n. We use formula $J = \lfloor \log_2(n) \rfloor$ to determine the finest level.

(S2) Calculate c_J. The boundary wavelets c_J consist of three parts, which we denote by c_J^X with $X \in \{L, I, R\}$. By definition $c_J^X = \langle f, \phi_J^X \rangle$. To calculate the inner product we cut f into pieces and approximate them though $f|_{2^{-J}[i,i+1]} \approx a_i + b_i x, i = 0, \cdots, 2^J - 1$. Noet that $\langle 1, \phi_J^X \rangle$ and $\langle x, \phi_J^X \rangle$ can be pre-calculated.

(S3) Decomposition. We can utilize (1) for direct computations of approximation involving boundary wavelets (only a few). As for the interior part, we use $c_{J-1} = c_J * a \downarrow 2$ same as the classical approach, where $*$ denotes convolution.

(S4) Thresholding. For this operation on the wavelet detail coefficients, we use the soft threshold method with predetermined thresholding parameters.

(S5) Reconstruction. For the boundary part, we utilize (1) for direct computations (only a few). As for the interior we use $c_J = (c_{J-1} \uparrow 2) * \tilde{a} + (d_{J-1} \uparrow 2) * \tilde{b}$.

Remark:*For the two-dimensional (or higher dimensional) case in Algorithm 1, we can perform a one-dimensional decomposition row by row and then column by column. In this way, we can avoid storing and calculating large matrices, which substantially improves the program's running efficiency. The computational complexity is proportional to the size of the data (linear complexity). In the image case f with size $m \times n$, we use $J = \lfloor \log_2(\min\{m, n\}) \rfloor$.*

We next discuss the ADMM algorithm to solve (5) with the bi-orthogonal boundary wavelets in Example 2. Note that the primal part of the scaling function is the hat function and thus $\Phi_x = I$, where I is the identity matrix. For ease of subsequent exposition, we denote the 2D-decomposition and reconstruction parts of Algorithm 1 as Dec2D() and Rec2D(), respectively. It is worth noting that since we are not dealing with c_{J_0} in the thresholding step, so we need set values of c_{J_0} to 0 in order to invoke the Rec2D(). In the Rec2D() we should use the same mask as in the Dec2D() instead of the primal part. The details is given in Algorithm 2.

Algorithm 2 ADMM for (5)

(S0) Initialization. Set the initial value of c, d and μ to 0. Choose the appropriate λ and ρ for subsequent iterations.
(S1) Update on c. Use the conjugate gradient method pcg to get an update on c. Define $f^{k+1} = 2^{J/2} f^k + \mathrm{Rec2D}(d^k - \mu^k)$. Thus, we have Rec2D(Dec2D(c^{k+1})) $= f^{k+1}$. We denote the process Rec2D(Dec2D()) as Trans(). Then we can apply the MATLAB code to get c^{k+1} = pcg(@Trans,f^{k+1}).
(S2) Update on d. Define $d^{k+0.5}$ = Dec2D(c^{k+1}) + μ^k, then $d^{k+1} = T_{\frac{\lambda}{\rho}}(d^{k+0.5})$.
(S3) Update on μ. Apply Dec2D() and we can get $\mu^{k+1} = \mu^k + \mathrm{Dec2D}(c^{k+1}) - d^{k+1}$.
(S4) Termination condition. Define t as a tolerance value, e.g., $t = 10^{-4}$. Iterative (S1)-S(3) until both $\|c^{k+1} - c^k\|_2 < t$ and $\|\mu^{k+1} - \mu^k\|_2 < t$ are satisfied.

IV. Numerical Experiments on Image Denoising

A. Numerical Results for Barbara

In this section, we take the classic 512×512 gray-scale images of *Barbara* as an example. To measure the quality of image restoration, we use peak-signal-to-noise ratio (PSNR). All the PSNR values are given after iterative convergence. The coarsest layer is 6 and the finest layer is 9. For noisy *Barbara*, 4 different approaches were considered:

1) **ADMM(BW)**: We use the ℓ_1 optimization model with ADMM integrated with our boundary wavelet system **BW**. Here for the soft-thresholding function $T_{\frac{\lambda}{\rho}}$ we take $\rho = 0.5$ and $\lambda = \tau\sigma/\sigma_0$, where $\tau = 3$ and $\sigma_0 = 5$.
2) **BW**: We directly utilize the boundary wavelet transform, apply the soft-thresholding operation on the detail coefficients once, and then reconstruct the image from the thresholded detail coefficients. The thresholding value is given by $T = 2^{-2J} \cdot c\sigma / \sqrt{|d|^2 - 2^{-2J}\sigma}$, where c is tuned to optimize the performance.
3) **ADMM(CW)**: Same as the ADMM(BW) in 1) but replace the BW system by CW system. All other parameters are the same for comparison purposes.
4) **CW**: Same as the BW in 2). We directly called the *wdenoise2* function in MATLAB using the CW system (i.e. *Bior2.2*). Here the thresholding method we use is *Bayes* and the thresholding rule we take is *Mean* to get the best PSNR value using this approach.

We can see Fig. 1 for the visual comparisons when $\sigma = 5$ and from Table I that the ℓ_1 optimization model with boundary wavelets through ADMM does show advantages over other methods in terms of PSNR, especially when the noise level is large ($\sigma \geq 25$). In conclusion, although applying boundary wavelets to the optimization model is more time-consuming compared to directly utilizing boundary wavelets for noise reduction, it does contribute to the effectiveness of the image denoising, which is well illustrated in TABLE I.

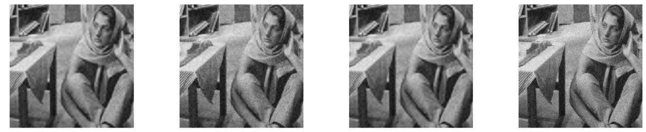

Fig. 1. Different Denoising Methods for *Barbara*. Left to Right: (1) AMDD+BW; (2) BW only; (3) ADMM+CW; (4) CW only.

TABLE I
Image Denoising Comparison Results of *Barbara*

Noise	**Different Methods for Denoising (PSNR)**				
σ	**Origin**	**ADMM(BW)**	**BW**	**ADMM(CW)**	**CW**
5	17.3784	23.4511	23.4025	**23.4569**	23.0623
10	14.6792	22.1209	**22.2489**	22.1251	21.3393
25	11.5201	**20.8579**	20.7418	20.8564	19.0287
40	10.1804	**19.9676**	19.7635	19.9672	17.8381
50	9.6242	**19.4685**	19.2621	19.4682	17.3051
80	8.6284	**18.3642**	18.1755	18.3641	16.2755

References

[1] C. K. Chui, *An introduction to wavelets*. Academic press, 1992, vol. 1.
[2] I. Daubechies, *Ten lectures on wavelets*. SIAM, 1992.
[3] B. Han, *Framelets and wavelets: Algorithms, Analysis, and Applications*. Springer, 2017.
[4] S. Mallat, *A wavelet tour of signal processing*. Elsevier, 1999.
[5] Y. Meyer, *Wavelets and operators: volume 1*. Cambridge University Press, 1992, no. 37.
[6] B. Han and X. Zhuang, "Analysis and construction of multivariate interpolating refinable function vectors," *Acta applicandae mathematicae*, vol. 107, no. 1-3, pp. 143–171, 2009.
[7] X. Zhuang, "Matrix extension with symmetry and construction of biorthogonal multiwavelets with any integer dilation," *Applied and Computational Harmonic Analysis*, vol. 33, no. 2, pp. 159–181, 2012.
[8] Z. Che and X. Zhuang, "Digital affine shear filter banks with 2-layer structure and their applications in image processing," *IEEE Transactions on Image Processing*, vol. 27, no. 8, pp. 3931–3941, 2018.
[9] Y. Meyer, "Ondelettes sur l'intervalle," *Revista Matematica Iberoamericana*, vol. 7, no. 2, pp. 115–133, 1991.
[10] A. Cohen, I. Daubechies, and P. Vial, "Wavelets on the interval and fast wavelet transforms," *Applied and computational harmonic analysis*, 1993.
[11] L. Andersson, N. Hall, B. Jawerth, and G. Peters, "Wavelets on closed subsets of the real line," *In21*, 1994.
[12] S. Grivet-Talocia and A. Tabacco, "Wavelets on the interval with optimal localization," *Mathematical Models and Methods in Applied Sciences*, vol. 10, no. 03, pp. 441–462, 2000.
[13] H. Harbrecht and R. Schneiderd, "Biorthogonal wavelet bases for the boundary element method," *Mathematische Nachrichten*, vol. 269, no. 1, pp. 167–188, 2004.
[14] W. Madych, "Finite orthogonal transforms and multiresolution analyses on intervals," *Journal of Fourier Analysis and Applications*, vol. 3, pp. 257–294, 1997.
[15] J. R. Williams and K. Amaratunga, "A discrete wavelet transform without edge effects using wavelet extrapolation," *Journal of Fourier analysis and Applications*, vol. 3, pp. 435–449, 1997.
[16] B. Han and Q. Jiang, "Multiwavelets on the interval," *Applied and Computational Harmonic Analysis*, vol. 12, no. 1, pp. 100–127, 2002.
[17] B. Han and M. Michelle, "Wavelets on intervals derived from arbitrary compactly supported biorthogonal multiwavelets," *Applied and Computational Harmonic Analysis*, vol. 53, pp. 270–331, 2021.
[18] S. H. Chan, X. Wang, and O. A. Elgendy, "Plug-and-play admm for image restoration: Fixed-point convergence and applications," *IEEE Transactions on Computational Imaging*, vol. 3, no. 1, pp. 84–98, 2016.